SCIENCE CHINA
Information Sciences

• RESEARCH PAPER •

October 2016, Vol. 59 102311:1–102311:17
doi: 10.1007/s11432-016-5555-3

Sinc interpolation based method for compensation of ionospheric dispersion effects on BOC signals with high subcarrier rate

Hang RUAN[1,2], Lei ZHANG[1,2*] & Teng LONG[1,2]

[1]*Key Laboratory of Electronic and Information Technology in Satellite Navigation* (*Beijing Institute of Technology*), *Ministry of Education, Beijing* 100081*, China;*
[2]*School of Information and Electronics, Beijing Institute of Technology, Beijing* 100081*, China*

Received July 7, 2015; accepted December 28, 2015; published online April 27, 2016

Abstract Binary Offset Carrier (BOC) signals with high subcarrier rate such as AltBOC(15,10) and cosBOC(15,2.5) have been adopted for the next generation of Global Navigation Satellite System (GNSS) to make full use of the allocated spectrum. However, the two main lobes of the BOC signals are tremendously separated in the frequency spectrum and the group delay of the two lobes are greatly dispersed due to ionospheric dispersion. The signals will suffer extremely severe distortion caused by the group delay dispersion including waveform ripples, power losses and correlation function asymmetries. In this paper, a novel time domain sinc interpolation based ionospheric dispersion compensation method is proposed to eliminate the distortion to the BOC signals. Firstly, the time domain model of BOC signal under the dispersive ionosphere is developed. Afterwards, based on the model, the two signal main lobes are aligned by sinc interpolation so that the ionospheric dispersion effects are almost mitigated. Taking Galileo E5 AltBOC(15,10) signal as an example, the performance of the proposed method is evaluated by simulation and test. The results show that the proposed method is able to more effectively compensate the ionospheric dispersion with fewer computational loads versus existing methods.

Keywords ionospheric dispersion, sinc interpolation, BOC, code tracking bias, high subcarrier rate

Citation Ruan H, Zhang L, Long T. Sinc interpolation based method for compensation of ionospheric dispersion effects on BOC signals with high subcarrier rate. Sci China Inf Sci, 2016, 59(10): 102311, doi: 10.1007/s11432-016-5555-3

1 Introduction

With the advent of the new global navigation satellite system (GNSS), such as BDS, Galileo and the modernized global positioning system (GPS) and GLONASS, binary offset carrier (BOC) modulations have been proposed to guarantee the coexistence and interoperability with different systems, improve the measurement precision and enhance the performance of multipath mitigation and interference rejection [1, 2]. Different from the traditional binary phase shift key (BPSK) signal, the square wave subcarrier in BOC signal divides the signal main lobe into two parts and moves them aside the existing GNSS signals. When the subcarrier rate is high, such as Galileo E5 AltBOC(15,10) and E1A cosBOC(15,2.5) signal [3],

* Corresponding author (email: aerolong@bit.edu.cn)

the frequency spacing between the two main lobes of the signal is really wide. In this case, the signal will suffer large group delay dispersion between the two main lobes when propagating across the ionosphere so that it cannot be regarded as a single tone signal [4]. However, the previous methods designed to receive BOC signal with high subcarrier rate such as general removing ambiguity via sidepeak suppression [5], dual estimate loop [6] and double phase estimator [7] all ignore the ionospheric effects. Although treating the signal as two BPSK signals can solve the problem [8], the advantages BOC signal brings are lost.

In [9], the detailed analysis of the ionospheric dispersion effects on AltBOC(15,10) signal is conducted by transforming the signal into frequency domain and shifting the signal phases of different frequency components according to the corresponding ionospheric delay. It shows that the dispersive ionosphere results in severe deformations and fluctuations of the time domain signals, power loss and asymmetry of the correlation function. As a result, the ionosphere dispersion compensation method is in great need or else the receiver performance will be highly degraded. At present, the existing method introduces the all-pass filter to compensate the dispersion but it requires extensive computations due to the high order filters and the complex coefficient calculation method [10]. Moreover, the ionosphere dispersion effects on BOC signal are analyzed with the frequency domain method and the expression of the ionosphere disturbed BOC signal in the time domain has not been studied yet.

In this paper, considering the fact that each main lobe of the BOC signal is more or less the same as the traditional BPSK signal which is usually treated as the single tone signal [11], the BOC signal with high subcarrier rate is modeled as the sum of the two main lobes. The time domain expression of the ionosphere distorted BOC signal is obtained by adjusting the delay of the two lobes according to the ionospheric dispersion effects. Based on the model, the time domain sinc interpolation based ionospheric dispersion compensation method is proposed which employs the interpolation before signal tracking to align the main lobes of the BOC signal. Taking Galileo E5 AltBOC(15,10) signal as an example, the effectiveness of the ionospheric dispersion compensation method is validated by the simulation that compares the time domain waveform, power loss and the correlation function asymmetries related code tracking bias with and without the compensation. The experiment using real Galileo E5 signal is also conducted for the validation. The results show that the proposed method is able to compensate the ionospheric dispersion effects more effectively with less computational loads versus the all-pass filter method.

The remainder of the paper is organized as follows. In Section 2, the BOC signals with high subcarrier rate used in new GNSS are summarized. The time domain model of the BOC signals under the dispersive ionosphere is developed in Section 3. Section 4 presents the proposed sinc interpolation based ionosphere compensation method. In Section 5, the performance of the proposed method is evaluated and compared with other methods by simulation and tests using real Galileo data. Section 6 concludes the paper.

2 BOC signal

BOC signals utilized in new GNSS adopt a subcarrier to shape the signal spectrum and improve the tracking performance. When the subcarrier is present, the satellite signal can be modeled as

$$y(t) = \sqrt{2C} s_{\mathrm{BOC}}(t-\tau_0)\cos(2\pi(f_{\mathrm{RF}}+f_d)t+\varphi_0), \tag{1}$$

where C, τ_0, f_d and φ_0 are the signal power, code delay, Doppler frequency and initial carrier phase respectively. f_{RF} is the center frequency of the GNSS signal. $s_{\mathrm{BOC}}(\cdot)$ is the pseudorandom sequence of BOC signal which is the pseudo random noise (PRN) code modulated by the square wave subcarrier. The navigation message or the secondary code is omitted for simplicity since the ionospheric dispersion effects on them are contained in the pseudorandom sequence. For cosBOC signal, $s_{\mathrm{BOC}}(\cdot)$ is

$$s_{\mathrm{BOC}}(t) = c(t)\mathrm{sgn}(\cos(2\pi f_{\mathrm{sc}}t)), \tag{2}$$

where f_{sc} is the subcarrier rate and $\mathrm{sgn}(x)$ is the symbol function which is 1 if $x \geqslant 0$ or else it is -1. $c(\cdot)$ is the PRN code. For AltBOC signal, the baseband signal with constant envelope is represented as [12]

$$s_{\mathrm{Alt}}(t) = (c_{aI}(t)+\mathrm{j}c_{aQ}(t))[\mathrm{sc}_a(t)+\mathrm{jsc}_a(t-T_{\mathrm{sc}}/4)] + (c_{bI}(t)+\mathrm{j}c_{bQ}(t))[\mathrm{sc}_a(t)-\mathrm{jsc}_a(t-T_{\mathrm{sc}}/4)]$$

$$+ (\overline{c_{aI}}(t) + \mathrm{j}\overline{c_{aQ}}(t))[\mathrm{sc}_p(t) + \mathrm{jsc}_p(t - T_{\mathrm{sc}}/4)] + (\overline{c_{bI}}(t) + \mathrm{j}\overline{c_{bQ}}(t))[\mathrm{sc}_p(t) - \mathrm{jsc}_p(t - T_{\mathrm{sc}}/4)], \quad (3)$$

where $\mathrm{sc}_a(t)$ and $\mathrm{sc}_p(t)$ are the subcarriers. T_{sc} is the subcarrier period which is $1/f_{\mathrm{sc}}$. c_{aI} and c_{bI} are the data signal components which are the navigation data modulated by the PRN code. c_{aQ} and c_{bQ} are the PRN codes of the pilot signal. $\overline{c_{aI}}$, $\overline{c_{aQ}}$, $\overline{c_{bI}}$ and $\overline{c_{bQ}}$ are the signal components which are used to obtain the constant envelope and contain no useful information. Due to the identical frequency spectrum, the ionospheric dispersion effects on the data signal are all the same as those on the pilot signal. Hence, only the pilot signal is considered in this paper for simplicity and the $s_{\mathrm{BOC}}(\cdot)$ of AltBOC signal is

$$s_{\mathrm{BOC}}(t) = [c_1(t) + c_2(t)]\mathrm{sc}_a(t) + \mathrm{j}[c_1(t) - c_2(t)]\mathrm{sc}_a(t - T_{\mathrm{sc}}/4), \quad (4)$$

where c_1 and c_2 are the PRN codes of c_{aQ} and c_{bQ} respectively. The cross correlation value between c_1 and c_2 is assumed to be zero since both of them are extracted from a family of quasiorthogonal codes. The expression of $\mathrm{sc}_a(t)$ is

$$\mathrm{sc}_a(t) = \sqrt{2}/4\mathrm{sgn}(\cos(2\pi f_{\mathrm{sc}}t - \pi/4)) + 1/2\mathrm{sgn}(\cos(2\pi f_{\mathrm{sc}}t)) + \sqrt{2}/4\mathrm{sgn}(\cos(2\pi f_{\mathrm{sc}}t + \pi/4)). \quad (5)$$

According to [6], when tracking the pilot channel of AltBOC signal, the local reference signal is $[c_1(t) + c_2(t)]\mathrm{sc}_a(t)$. Since the correlation between $c_1(t) + c_2(t)$ and $c_1(t) - c_2(t)$ is zero, the imaginary part of the correlation result between $s_{\mathrm{BOC}}(t)$ and the local reference is zero. Hence, the imaginary part of $s_{\mathrm{BOC}}(t)$ is omitted and the pseudorandom sequence of AltBOC signal is simplified as

$$s_{\mathrm{BOC}}(t) = [c_1(t) + c_2(t)]\mathrm{sc}_a(t). \quad (6)$$

Considering sc_a is a four-level signal which has the waveform similar to cosine function, the pseudorandom sequence expressions of cosBOC and AltBOC signal are unified as below

$$s_{\mathrm{BOC}}(t) = 1/L[c_1(t) + c_2(t)]\mathrm{SC}_{\cos}(t), \quad (7)$$

where c_1 is equal to c_2 and L is 1/2 for cosBOC signal. For AltBOC signal, L is 1. $\mathrm{SC}_{\cos}(t)$ represents the subcarrier which is $\mathrm{sgn}(\cos(2\pi f_{\mathrm{sc}}t))$ for cosBOC signal and $\mathrm{sc}_a(t)$ for AltBOC signal. The Doppler frequency shift of the code and subcarrier is not considered since they can be recovered by the carrier tracking loops [13].

3 Time domain ionospheric dispersion signal model

The ionosphere is dispersive in which higher frequency components of the signal propagate faster than lower frequency components. Consequently, when signals pass through the ionosphere, different frequency components suffer different delay. Usually, the ionosphere's frequency dependent group delay is simply modeled as [14]

$$\tau_{\mathrm{i}}(f) = \frac{40.3\ \mathrm{TEC}}{v_c \cdot f^2}, \quad (8)$$

where v_c (m/s) is the vacuum speed of light and f (Hz) is the frequency of the transmitted signals. TEC (electrons/m^2) is the line integral of the free electron density along the direct ray path. For the traditional GPS L1 C/A signal with the narrow bandwidth, the delay of different frequencies within the signal bandwidth varies a little so that the signal can be simplified as a single tone signal.

In order to make use of the greatly separated band in frequency spectrum, BOC signals with high subcarrier rate are used in new GNSS such as Galileo E5 AltBOC(15,10) and E1A cosBOC(15,2.5) whose subcarrier rate is as large as 15.345 MHz. The power spectral densities of AltBOC(15,10) and cosBOC(15,2.5) signal are shown in Figure 1 [15]. The total bandwidth of the signals is really large because of the greatly separated main lobes and the group delay induced by ionosphere varies a lot within the signal bandwidth. Therefore, the signal cannot be treated as a single tone signal when traveling across the ionosphere [9]. Furthermore, as the relationship between the group delay of ionosphere and signal frequency is non-linear, the time domain expression of the signal is difficult to be calculated directly.

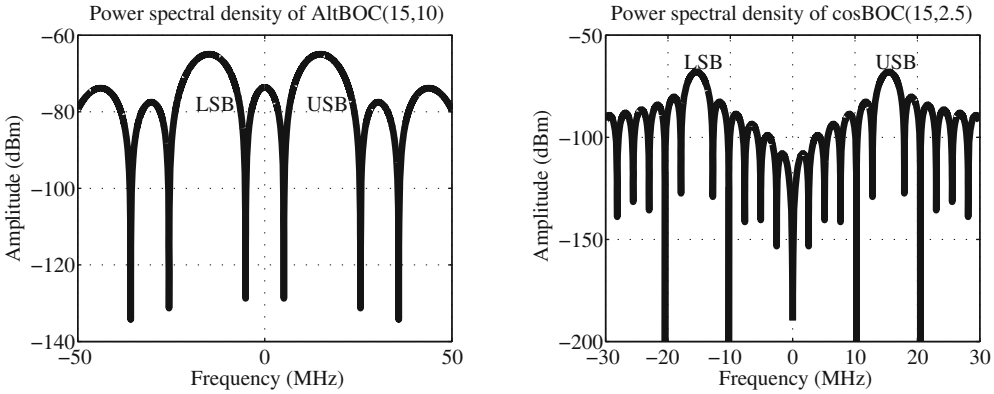

Figure 1 The power spectral density of AltBOC(15,10) and cosBOC(15,2.5).

However, the two main lobes of BOC signal are derived from the modulation of $\mathrm{SC}_{\cos}(t)$. In GNSS, the signals transmitted by the satellites are usually bandlimited. Moreover, the filter of the receiver frontend removes high-frequency signal components. As a result, the subcarrier can be approximated as

$$\mathrm{SC}_{\cos}(t) \approx \cos(2\pi f_{\mathrm{sc}} t). \tag{9}$$

In this case, each of the two main lobes is the traditional BPSK signal with a relatively narrow bandwidth and both of them can be regarded as a single tone signal according to NeQuick model which hardly brings any error [16]. As a result, the BOC signal deformed by the ionosphere is modeled as the sum of the two main lobes with different delay. If the main lobe with higher frequency is regarded as up side band (USB) signal and that with lower frequency is regarded as low side band (LSB) signal as shown in Figure 1, the power normalized USB signal $y_u(t)$ and LSB signal $y_l(t)$ are present based on the model (1) as below

$$y_u(t) = s_{\mathrm{USB}}(t - \tau_0 - \tau_u)\cos(2\pi(f_{\mathrm{RF}} + f_d)t + \varphi_0 + \varphi_u), \tag{10}$$

$$y_l(t) = s_{\mathrm{LSB}}(t - \tau_0 - \tau_l)\cos(2\pi(f_{\mathrm{RF}} + f_d)t + \varphi_0 + \varphi_l), \tag{11}$$

where τ_u and τ_l are the ionospheric delay of the USB and LSB signal which are equal to the ionospheric delay at the USB and LSB center frequency respectively. φ_u and φ_l are the ionosphere induced carrier phase variation of the USB and LSB signal. $s_{\mathrm{USB}}(\cdot)$ and $s_{\mathrm{LSB}}(\cdot)$ are the pseudorandom sequences of the USB and LSB signal which are

$$s_{\mathrm{USB}}(t) = 1/Lc_1(t)(\mathrm{SC}_{\cos}(t) + \mathrm{jSC}_{\cos}(t - T_{\mathrm{sc}}/4)), \tag{12}$$

$$s_{\mathrm{LSB}}(t) = 1/Lc_2(t)(\mathrm{SC}_{\cos}(t) - \mathrm{jSC}_{\cos}(t - T_{\mathrm{sc}}/4)). \tag{13}$$

The time domain expression $y_i(t)$ of the ionospheric dispersion deformed BOC signal is

$$y_i(t) = y_u(t) + y_l(t). \tag{14}$$

When there is no ionospheric dispersion, τ_u is equal to τ_l and φ_u is equal to φ_l. In this instance, the expression is the same as (1).

Since the correlation result of the pseudorandom sequence can indicate most of the disturbance on BOC signal brought by ionosphere, also the positioning of GNSS receiver is based on the satellite pseudo ranges extracted from the correlation result, the cross correlation function (CCF) between the BOC signals with and without ionospheric dispersion is calculated to further verify the correctness of the time domain model (10)(11). According to (12-14), the pseudorandom sequence of the ionospheric dispersion deformed BOC signal is $s_{\mathrm{USB}}(t - \tau_u) + s_{\mathrm{LSB}}(t - \tau_l)$ and the expression of the CCF $R_d(\tau)$ is

$$\begin{aligned} R_d(\tau) &= \frac{1}{T_c}\int_0^{T_c} (s_{\mathrm{USB}}(t - \tau_u) + s_{\mathrm{LSB}}(t - \tau_l))s_{\mathrm{BOC}}(t - \tau)\mathrm{d}t \\ &= \left[\frac{1}{L}R_{\mathrm{BOC},c_1}(\tau - \tau_u) + \frac{1}{L}R_{\mathrm{BOC},c_2}(\tau - \tau_l)\right] + \mathrm{j}\left[\frac{1}{L}R_{\mathrm{SC},c_1}(\tau - \tau_u) - \frac{1}{L}R_{\mathrm{SC},c_2}(\tau - \tau_l)\right], \end{aligned} \tag{15}$$

where

$$R_{\mathrm{BOC},c_1}(\tau)=\frac{1}{T_c}\int_0^{T_c}c_1(t)\mathrm{SC}_{\cos}(t)c_1(t-\tau)\mathrm{SC}_{\cos}(t-\tau)\mathrm{d}t,$$
$$R_{\mathrm{BOC},c_2}(\tau)=\frac{1}{T_c}\int_0^{T_c}c_2(t)\mathrm{SC}_{\cos}(t)c_2(t-\tau)\mathrm{SC}_{\cos}(t-\tau)\mathrm{d}t,$$
$$R_{\mathrm{SC},c_1}(\tau)=\frac{1}{T_c}\int_0^{T_c}c_1(t)\mathrm{SC}_{\cos}(t)c_1(t-\tau)\mathrm{SC}_{\cos}(t-\tau-T_{\mathrm{sc}}/4)\mathrm{d}t,$$
$$R_{\mathrm{SC},c_2}(\tau)=\frac{1}{T_c}\int_0^{T_c}c_2(t)\mathrm{SC}_{\cos}(t)c_2(t-\tau)\mathrm{SC}_{\cos}(t-\tau-T_{\mathrm{sc}}/4)\mathrm{d}t.$$

T_c is the pseudorandom sequence period. As c_1 and c_2 are equivalent PRN codes and their autocorrelation functions (ACF) are identical for both the AltBOC and cosBOC signal, $R_{\mathrm{BOC},c_1}(\tau)$ and $R_{\mathrm{BOC},c_2}(\tau)$ are unified as $R_{\mathrm{BOC}}(\tau)$ and $R_{\mathrm{SC},c_1}(\tau)$ and $R_{\mathrm{SC},c_2}(\tau)$ are unified as $R_{\mathrm{SC}}(\tau)$ whose expressions are

$$\begin{aligned}R_{\mathrm{BOC}}(\tau)&=\frac{1}{T_c}\int_0^{T_c}c(t)\,\mathrm{SC}_{\cos}(t)\,c(t-\tau)\,\mathrm{SC}_{\cos}(t-\tau)\,\mathrm{d}t\\&=\sum_{i=2-M}^{M-2}(-1)^i\cdot\left(1-i\frac{T_{\mathrm{sc}}}{2T_p}\right)\mathrm{tri}_{T_{\mathrm{sc}}}\left(\tau-i\cdot\frac{T_{\mathrm{sc}}}{2}\right)\\&\quad+\sum_{k=0}^{1}(-1)^M\cdot\frac{T_{\mathrm{sc}}}{4T_p}\mathrm{tri}_{\frac{T_{\mathrm{sc}}}{2}}\left(\tau-(-1)^k\left(T_p-\frac{T_{\mathrm{sc}}}{4}\right)\right)\\&\quad+\sum_{k=0}^{1}(-1)^{M-1}\cdot\frac{T_{\mathrm{sc}}}{2T_p}\mathrm{tri}_{\frac{T_{\mathrm{sc}}}{2}}\left(\tau-(-1)^k\left(T_p-\frac{T_{\mathrm{sc}}}{2}\right)\right)P_{\frac{T_{\mathrm{sc}}}{4}}\left(\tau-(-1)^k\left(T_p-\frac{T_{\mathrm{sc}}}{2}\right)\right)\\&\quad+\sum_{k=0}^{1}(-1)^{M-1}\cdot\frac{T_{\mathrm{sc}}}{2T_p}\mathrm{tri}_{T_{\mathrm{sc}}}\left(\tau-(-1)^k\left(T_p-\frac{T_{\mathrm{sc}}}{2}\right)\right)P_{\frac{T_{\mathrm{sc}}}{2}}\left(\tau-(-1)^k\left(T_p-T_{\mathrm{sc}}\right)\right),\end{aligned}\tag{16}$$

$$\begin{aligned}R_{\mathrm{SC}}(\tau)&=\frac{1}{T_c}\int_0^{T_c}c(t)\mathrm{SC}_{\cos}(t)c(t-\tau)\mathrm{SC}_{\cos}(t-\tau-T_{\mathrm{sc}}/4)\mathrm{d}t\\&=\sum_{i=-M}^{M-1}(-1)^{i+1}[2(M-\mathrm{sgn}(i)\cdot i)-\mathrm{sgn}(i)]\frac{T_{\mathrm{sc}}}{4T_p}\cdot\mathrm{tri}_{\frac{T_{\mathrm{sc}}}{2}}\left(\tau-i\frac{T_{\mathrm{sc}}}{2}-\frac{T_{\mathrm{sc}}}{4}\right),\end{aligned}\tag{17}$$

where c represents c_1 and c_2. $\mathrm{tri}_T(\cdot)$ is the triangle function with the width of T, peak amplitude of 1 and center of zero. $P_T(\cdot)$ is the square pulse function with the width of T, amplitude of 1 and it starts at the time of zero. T_p is the code chip duration. M is $2T_p/T_{\mathrm{sc}}$.

Figure 2 illustrates the normalized ionospheric dispersion distorted CCF of AltBOC(15,10) and cosBOC(15,2.5) signal calculated from (15) when TEC is 50 TECU. The CCF calculated with the frequency domain method in [9] is also drawn in the figure together with the ideal ACF without any ionospheric dispersion for comparison and verification. It shows that the peaks of the CCF with ionospheric dispersion are delayed, attenuated, deformed in contrast to the ideal ACF. The dispersive ionosphere also creates the imaginary part in the correlation function. Accordingly, the receiver performance will degrade a lot if the total band of BOC signal is directly processed without ionosphere compensation. In addition, the ionospheric dispersion distorted CCF of AltBOC(15,10) and cosBOC(15,2.5) calculated from (15) are probably the same as those calculated with the frequency domain method. In order to evaluate the difference between the correlation functions calculated from the two methods in the condition of different TEC, the mean deviation E_{tf} is designed as below which computes the mean value of the difference between the correlation function of (15) and that obtained with the frequency domain method in the delay of ±1 chip relative to the maximum peak value P_{R_d} of the real part of $R_d(\tau)$

$$E_{tf}=\frac{1}{2T_p\cdot P_{R_d}}\int_{-T_p}^{T_p}|\Im\{R_d(\tau)\}-\Im\{R_{f,i}(\tau)\}|\mathrm{d}\tau,\tag{18}$$

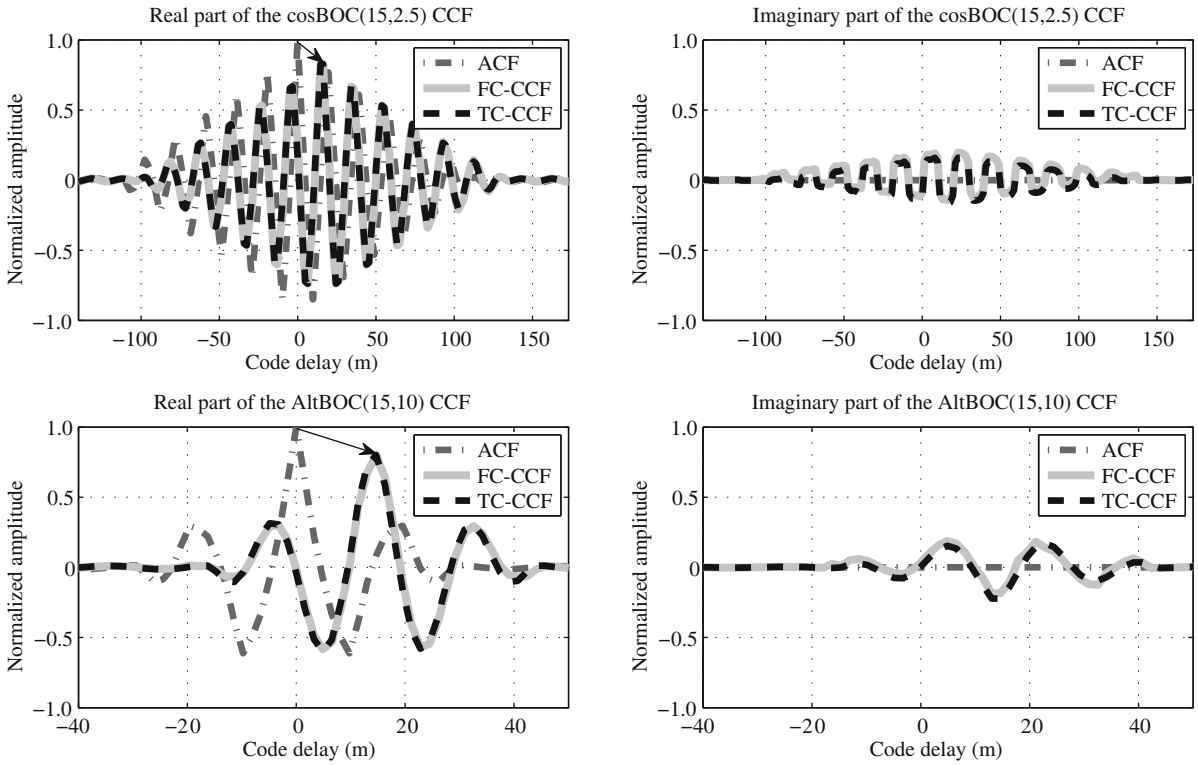

Figure 2 The real part and imaginary part of the CCF between the BOC signals with and without ionospheric dispersion. FC represents it is calculated with the frequency domain method and TC represents it is calculated from (15).

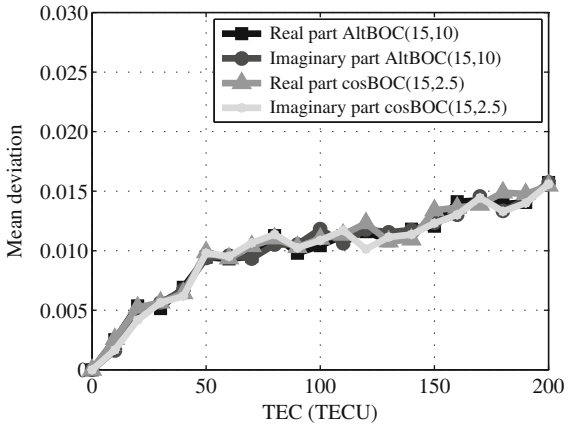

Figure 3 The mean deviation between CCF (15) and that calculated from the frequency domain method.

where $R_{f,i}(\cdot)$ is the correlation function calculated with the frequency domain method. $\Im\{x\}$ is the operator that calculates the real part or imaginary part of x corresponding to computing the mean deviation of the CCF real part and imaginary part respectively. The range of ± 1 chip is the valid area for the correlation of the PRN code. The mean deviation of the real part and imaginary part of the CCF is illustrated for AltBOC(15,10) and cosBOC(15,2.5) signal in Figure 3.

It is clear that the mean deviations for the two signals are both less than 0.015 when TEC ranges from 0 TECU to 200 TECU which are the typical cases on earth. As the frequency domain method is derived from the ionosphere model without approximation, the designed time domain model is proper for the study of the ionospheric dispersion effects on the correlation function. Furthermore, the results validate the assumption that the BOC signal with high subcarrier rate can be regarded as the sum of the two main lobes. Each of the main lobes is treated as the single tone signal whose ionospheric delay is equal to that at the center frequency of the lobe.

4 Sinc interpolation based ionospheric dispersion compensation method

It is known that, when there is no ionosphere, processing the entire band of the BOC signal with high subcarrier rate greatly outperforms the single-band and separate dual-band method. Accordingly, the ionospheric dispersion should be compensated to avoid the waveform ripples, power loss and correlation function asymmetries. Based on the time domain model designed above, it can be realized by adjusting the phases of the two BOC signal's main lobes. However, in GNSS receiver, the incoming down-converted satellite signal is digitalized in a fixed relatively low sampling rate to reduce complexity. Taking Galileo E5 AltBOC(15,10) signal as an example, the signal bandwidth is 51.15 MHz so that the sampling rate is generally around 110 MHz. In this case, shifting one sampling point will lead to the time variation of 9.1 ns. The group delay dispersion between the two main lobes due to ionosphere ranges from 0.4 ns to 3.2 ns when TEC varies from 10 TECU to 100 TECU. For cosBOC(15,2.5) signal, the result is probably the same. Hence, the ionospheric dispersion cannot be effectively compensated by the only movement of the intact sampling points and the digital signals have to be time shifted within the sampling period.

In signal processing, interpolation method is able to calculate the signal value of the point between the original sampling data. As a result, it is employed to adjust the relative phases of the two main lobes of BOC signal so as to compensate the undesired phase shifts that arisen by the ionospheric dispersion.

4.1 Sinc interpolation method

Before describing the procedure of the interpolation for the ionospheric dispersion compensation, this subsection first reviews the interpolation methods. In the previous study, several interpolation methods have been proposed including the Lagrange interpolation [17], time domain sinc interpolation [18] and frequency sinc interpolation [19], etc. All of the methods can achieve the time shift within the sampling period for digital signal. In consideration of the computational loads and the discrete periodic property of GNSS digital signal, time domain sinc interpolation shows better performance [20].

Let $x(nT_s)$ be a sequence of a uniformly sampled band limited signal $x(t)$ where T_s is the sampling period such that $1/T_s$ is larger than twice the highest frequency of $x(t)$. The sinc interpolation of the sequence is given by the infinite sum

$$x(t) = \sum_{n=-\infty}^{\infty} x(nT_s)\mathrm{sinc}(\pi(t-nT_s)/T_s) = \sum_{n=-\infty}^{\infty} x(nT_s)\frac{\sin(\pi(t-nT_s)/T_s)}{(\pi(t-nT_s)/T_s)}, \tag{19}$$

where the sinc function is the interpolation kernel. The interpolation is the convolution between $x(nT_s)$ and the sinc function so that the result in the frequency domain is the product of the discrete signal and the square function with the band edge of $\pm 1/2T_s$. Therefore, the continuous signal is filtered out and the signal value of any time can be calculated. Nevertheless, it is unrealizable due to the infinite length of the summation. Thus, it is simplified into the finite sums as below [18]

$$x(t) = \sum_{n=-L}^{M-1} x(nT_s)\frac{\sin(\pi(t-nT_s)/T_s)}{(\pi(t-nT_s)/T_s)}, \tag{20}$$

where L and M are arbitrary integers that obey the relation $L+M=N$. N is the size of the interpolation kernel. As Gibbs phenomenon is normally associated with the truncated interpolation kernel, the accuracy of the signal value calculated by interpolation may be distorted. In order to diminish the distortion, the windowed sinc interpolation is introduced as below

$$x(t) = \sum_{n=-L}^{M-1} x(nT_s)\frac{\sin(\pi(t-nT_s)/T_s)}{(\pi(t-nT_s)/T_s)}w(t-nT_s), \tag{21}$$

where $w(\cdot)$ is the window function. It is usually the Blackman window or Kaiser window that is declared to be the top performers for the restraint of the Gibbs phenomenon in interpolation [21]. As a result, the signal value of any time instant within the digitalized signal sampling interval can be recovered with high accuracy which will help a lot for the ionospheric dispersion compensation.

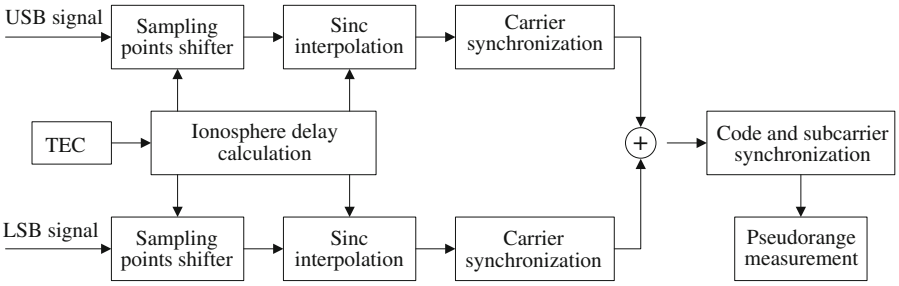

Figure 4 The block schematic diagram of sinc interpolation based ionospheric dispersion compensation method.

4.2 Dispersion compensation method

Based on the coherent dual-band receiver architecture described in [22], the block schematic diagram of the proposed sinc interpolation based ionospheric dispersion compensation method is shown in Figure 4. The input BOC signal is divided into the USB and LSB signal corresponding to the main lobes with high frequency and low frequency respectively and sent into two signal processing channels. Both of the USB and LSB signal are digitalized intermediate frequency signals which are synchronously sampled. The ionosphere delay of each side band signal is calculated from (8) based on the real-time monitored/forecasted TEC. The block of sampling point shifter adjusts the signal phase in the unit of sampling period and the sinc interpolation adjusts the signal phase within the sampling interval according to the ionosphere delay. Afterwards, the carriers of the two side band signals are synchronized independently with the help of two phase lock loops (PLL). The frequency of the local carriers is the center frequency of the input BOC signal. Finally, the two side bands are added together to rebuild the BOC signal. A subcarrier lock loop (SLL) and a delay lock loop (DLL) are used to track the pseudorandom sequence of the BOC signal. The pseudorange measurement is gained from the correlation results.

As the paper concentrates on the ionospheric dispersion effects, the noise component is omitted for simplicity. The USB and LSB signal after down converted and digitalized at the sampling rate $f_s = 1/T_s$ are expressed below

$$y_{\mathrm{USB}}(nT_s) = \sqrt{C}s_{\mathrm{USB}}(nT_s - \tau_0 - \tau_u)\cos(2\pi(f_{\mathrm{IF}} + f_d)nT_s + \varphi_0 + \varphi_u), \tag{22}$$

$$y_{\mathrm{LSB}}(nT_s) = \sqrt{C}s_{\mathrm{LSB}}(nT_s - \tau_0 - \tau_l)\cos(2\pi(f_{\mathrm{IF}} + f_d)nT_s + \varphi_0 + \varphi_l), \tag{23}$$

where f_{IF} is the signal intermediate frequency which fulfills the conditions [23]

$$f_{\mathrm{IF}} > 0.5B_n, \quad f_s > 2 \times (f_{\mathrm{IF}} + 0.6B_n), \tag{24}$$

where B_n is the bandwidth of the signal. The sampling rate is a little larger than the standard Nyquist sampling rate so as to reduce the sampling loss. In the following, the effects of quantization are neglected and it is assumed that the signal is sampled without introducing significant distortions.

Since the sampling period is much larger than the difference between the ionosphere delay of the two main lobes that should be compensated as the statement above, τ_u and τ_l are rewritten as below

$$\tau_u = k_u T_s + \Delta\tau_u, \tag{25}$$

$$\tau_l = k_l T_s + \Delta\tau_l, \tag{26}$$

where k_u and k_l are the integer number of sampling periods in the ionosphere delay. $\Delta\tau_u$ and $\Delta\tau_l$ are the residuals within the sampling period. The components $k_u T_s$ and $k_l T_s$ can be compensated by shifting the sampling points in time domain. The two side band signals after shifting k_u and k_l sampling points respectively are

$$y_{\mathrm{USB}}(nT_s + k_u T_s) = \sqrt{C}s_{\mathrm{USB}}(nT_s - \tau_0 - \Delta\tau_u)\cos(2\pi(f_{\mathrm{IF}} + f_d)(n + k_u)T_s + \varphi_0 + \varphi_u), \tag{27}$$

$$y_{\mathrm{LSB}}(nT_s + k_l T_s) = \sqrt{C}s_{\mathrm{LSB}}(nT_s - \tau_0 - \Delta\tau_l)\cos(2\pi(f_{\mathrm{IF}} + f_d)(n + k_l)T_s + \varphi_0 + \varphi_l). \tag{28}$$

For simplicity, $y_{\mathrm{USB}}[n]$ and $y_{\mathrm{LSB}}[n]$ are used to denote the discrete time sequences $y_{\mathrm{USB}}(nT_s+k_uT_s)$ and $y_{\mathrm{LSB}}(nT_s+k_lT_s)$. Subsequently, sinc interpolation is utilized to calculate the $y_{\mathrm{USB}}(nT_s+k_uT_s+\Delta\tau_u)$ and $y_{\mathrm{LSB}}(nT_s+k_lT_s+\Delta\tau_l)$ from the discrete digital sequences as below

$$y_{\mathrm{USB}}(nT_s+k_uT_s+\Delta\tau_u)=\frac{1}{S_u}\sum_{k=-L}^{M-1}y_{\mathrm{USB}}[n+k]\frac{\sin(\pi(\Delta\tau_u-kT_s)/T_s)}{\pi(\Delta\tau_u-kT_s)/T_s}, \tag{29}$$

$$y_{\mathrm{LSB}}(nT_s+k_lT_s+\Delta\tau_l)=\frac{1}{S_l}\sum_{k=-L}^{M-1}y_{\mathrm{LSB}}[n+k]\frac{\sin(\pi(\Delta\tau_l-kT_s)/T_s)}{\pi(\Delta\tau_l-kT_s)/T_s}, \tag{30}$$

where S_u and S_l are the normalization coefficients as

$$S_x=\sum_{k=-L}^{M-1}\frac{\sin(\pi(\Delta\tau_x-kT_s)/T_s)}{\pi(\Delta\tau_x-kT_s)/T_s}, \tag{31}$$

where x is u or l corresponding to the USB and LSB signal respectively. The original sampling points used for the interpolation calculation are those aside the interpolation point. As the interpolation kernel size N is even, the number of sampling points on both sides of the interpolation point is the same which is $N/2$. Then, L is $N/2-1$ and M is $N/2+1$. The interpolation results are

$$y_{\mathrm{USB}}(nT_s+k_uT_s+\Delta\tau_u)=\frac{\sin(\pi\Delta\tau_u/T_s)}{S_uN}\sum_{k=1-N/2}^{N/2}y_{\mathrm{USB}}[n+k](-1)^k\cot[\pi(\Delta\tau_u-kT_s)/NT_s], \tag{32}$$

$$y_{\mathrm{LSB}}(nT_s+k_lT_s+\Delta\tau_l)=\frac{\sin(\pi\Delta\tau_l/T_s)}{S_lN}\sum_{k=1-N/2}^{N/2}y_{\mathrm{LSB}}[n+k](-1)^k\cot[\pi(\Delta\tau_l-kT_s)/NT_s]. \tag{33}$$

Referring to (22) and (23), the $s_{\mathrm{USB}}(\cdot)$ and $s_{\mathrm{LSB}}(\cdot)$ in $y_{\mathrm{USB}}(nT_s+k_uT_s+\Delta\tau_u)$ and $y_{\mathrm{LSB}}(nT_s+k_lT_s+\Delta\tau_l)$ are synchronous from each other so that the codes and subcarriers of the two bands are aligned. However, the ionosphere disperses the carrier phase to the opposite direction and the interpolation processing even enlarges the separation between the carrier phases of the two bands. Thus, the carrier of each side band has to be synchronized independently. By using two PLLs, the carrier synchronization processing of the two side bands are

$$y_{B,u}[n]=y_{\mathrm{USB}}(nT_s+k_uT_s+\Delta\tau_u)\exp[\mathrm{j}(2\pi(f_{\mathrm{IF}}+f_d)(n+k_u)T_s+\varphi_0+\varphi'_u)], \tag{34}$$

$$y_{B,l}[n]=y_{\mathrm{LSB}}(nT_s+k_lT_s+\Delta\tau_l)\exp[\mathrm{j}(2\pi(f_{\mathrm{IF}}+f_d)(n+k_l)T_s+\varphi_0+\varphi'_l)], \tag{35}$$

where $y_{B,u}[n]$ and $y_{B,l}[n]$ are the baseband discrete time sequences of the USB and LSB signal. φ'_u and φ'_l are the estimated carrier phase residuals calculated from the PLL of each side band which are

$$\varphi'_u=\varphi_u+\Delta\varphi_u, \tag{36}$$

$$\varphi'_l=\varphi_l+\Delta\varphi_l, \tag{37}$$

where $\Delta\varphi_u$ and $\Delta\varphi_l$ are interpolation induced carrier phase shift of the USB and LSB signal. Then, the two side bands are added to form the ionosphere compensated baseband BOC signal $y_s[n]$ as below

$$y_s[n]=y_{B,u}[n]+y_{B,l}[n]. \tag{38}$$

It is correlated with the local reference subcarrier and code signals. If the coherent integration length is set as T_c, the final correlation output $y_o(kT_c)$ is gained as below

$$\begin{aligned}y_o(kT_c)&=\frac{T_s}{T_c}\sum_{n=(k-1)T_c/T_s}^{kT_c/T_s-1}y_s[n]s_{\mathrm{BOC}}(nT_s-\tau'_0)\\&=\sqrt{C}\mathrm{sinc}(\pi\Delta f_dT_c)[R_{\mathrm{USB}}(\tau)\exp(\mathrm{j}\varphi_U)+R_{\mathrm{LSB}}(\tau)\exp(\mathrm{j}\varphi_L)],\end{aligned} \tag{39}$$

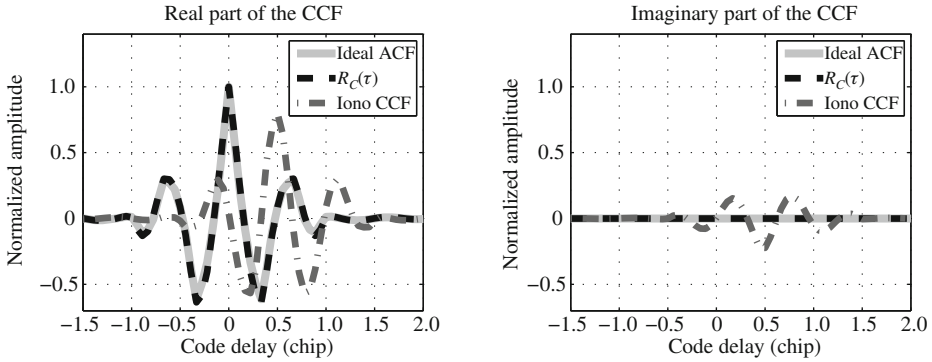

Figure 5 Correlation result of sinc interpolation based ionospheric dispersion compensation.

where Δf_d is the Doppler frequency error, τ_0' is the estimated code phase and $\tau = \tau_0' - \tau_0$. $R_{\rm USB}(\tau)$ and $R_{\rm LSB}(\tau)$ are the CCF between the ideal BOC signal and the ionosphere compensated USB and LSB signal respectively. φ_U and φ_L are the carrier tracking error of the two side band signals. Because the carriers of the two side bands are tracked independently by two PLLs, each of them is the same as the carrier phase synchronization of the traditional narrow band BPSK signal which is free of the dispersion induced by ionosphere and interpolation [23]. Consequently, the carrier tracking error is really small so that it is assumed zero and the correlation output is

$$y_o(kT_c) = \sqrt{C}R_C(\tau) = \sqrt{C}[R_{\rm USB}(\tau) + R_{\rm LSB}(\tau)], \tag{40}$$

where $R_C(\tau)$ is the CCF between the ionosphere compensated BOC signal and the ideal BOC signal.

Considering the ionospheric dispersion effects on AltBOC and other BOC signals with high subcarrier rate are similar, the following analysis is based on Galileo E5 AltBOC(15,10) signal as an example. The normalized CCF of Galileo E5 AltBOC(15,10) signal after ionosphere compensation is shown in Figure 5. The sampling rate is 120 MHz and the TEC is 50 TECU. The interpolation kernel size is 8. The ideal ACF without any ionospheric dispersion and the correlation function with ionospheric dispersion are drawn for comparison. It shows that the deformation, peak delay and power attenuation is significantly diminished and the CCF of the signal after ionosphere compensation is nearly all the same as the ideal ACF which claims that the sinc interpolation based method can perfectly compensate the ionospheric dispersion.

In order to further improve the accuracy of the ionospheric dispersion compensation, windowed interpolation is utilized to reduce the Gibbs phenomena as stated in the last subsection [21]. The USB and LSB signal after the windowed interpolation are

$$y_{\rm USB}(nT_s + k_uT_s + \Delta\tau_u) = \frac{\sin(\pi\Delta\tau_u/T_s)}{S_{u,w}N} \sum_{k=1-N/2}^{N/2} y_{\rm USB}[n+k](-1)^k \cot[\pi(\Delta\tau_u - kT_s)/NT_s]w(\Delta\tau_u - kT_s), \tag{41}$$

$$y_{\rm LSB}(nT_s + k_lT_s + \Delta\tau_l) = \frac{\sin(\pi\Delta\tau_l/T_s)}{S_{l,w}N} \sum_{k=1-N/2}^{N/2} y_{\rm LSB}[n+k](-1)^k \cot[\pi(\Delta\tau_l - kT_s)/NT_s]w(\Delta\tau_l - kT_s), \tag{42}$$

where $S_{u,w}$ and $S_{l,w}$ are the normalization coefficients of the windowed sinc interpolation in the USB and LSB signal which are the sum of the interpolation kernel. After the windowed interpolation, the following signal processing is the same as that without windowed. When TEC is 50 TECU, the interpolation kernel size is 8 and the window function is the Blackman window, the normalized CCF is drawn in Figure 6. Compared with the result without windowed, the signal is more accurately recovered from the ionospheric dispersion especially the sharp peaks in the correlation result.

In addition, the interpolation kernel size can be increased to further improve the compensation performance. As the correlation result plays an important role in the position calculation of GNSS receiver, the

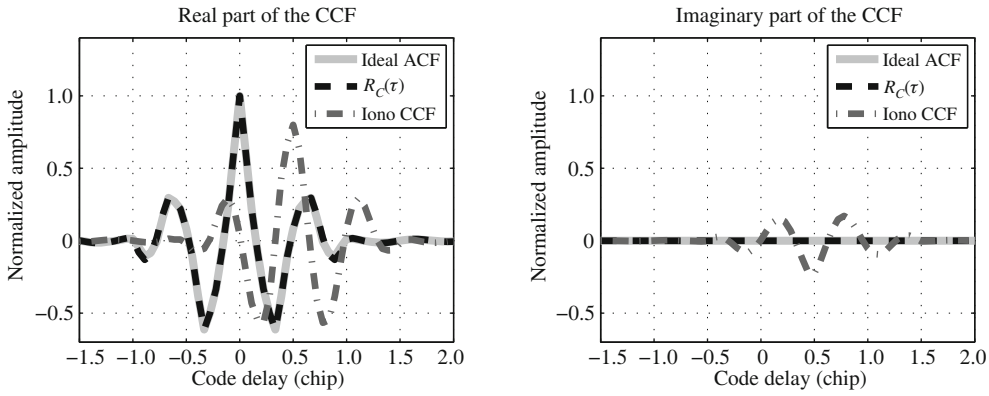

Figure 6 Correlation result of windowed sinc interpolation based ionospheric dispersion compensation.

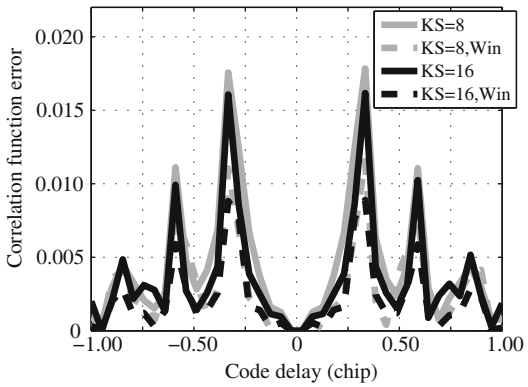

Figure 7 The difference between the compensated correlation function and the ideal ACF. Win represents the interpolation is Blackman windowed. KS is short for kernel size. TEC = 50 TECU.

difference between $R_C(\tau)$ and the ideal ACF $R_a(\tau)$ without any ionospheric dispersion is calculated to confirm the interpolation kernel size and whether the window function is needed or not. The expression of the difference is as below where P_{R_a} is the maximum value of $R_a(\tau)$.

$$D_{I-C}(\tau) = \frac{1}{P_{R_a}}|R_a(\tau) - R_C(\tau)|. \tag{43}$$

The results for the code delay ranging from -1 chip to 1 chip are drawn in Figure 7. It shows that, even for the non-windowed interpolation with the kernel size of 8, the maximum difference is smaller than 0.02 relative to the maximum peak value of the correlation results. Accordingly, it is further concluded that the sinc interpolation based method is able to successfully compensate the ionospheric dispersion. Furthermore, the error is approximately symmetric to the code delay of zero so that the symmetry of the correlation result is better kept. As the code is synchronized with the help of the symmetry [13], the code tracking bias will be reduced. In addition, the window function plays a more important role in the improvement of the ionospheric dispersion compensation accuracy. In consideration of the computational loads, the Blackman windowed sinc interpolation with the kernel size of 8 is utilized and evaluated in the next section since the difference between the sinc interpolation kernel sizes of 8 and 16 is little.

5 Performance evaluation

In this section, the performance of the proposed sinc interpolation based ionospheric dispersion compensation method is evaluated by simulation and test using real Galileo data. Based on the analysis above, the Blackman windowed sinc interpolation with the size of 8 is chosen as an example for the evaluation since it gains the tradeoff between the computational loads and compensation accuracy. The time domain waveform, power loss and code tracking bias are compared in the assessment. The complexity of

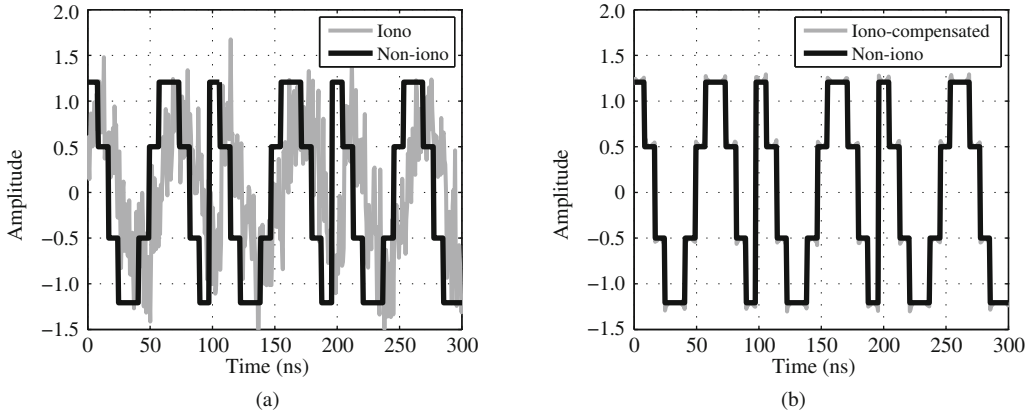

Figure 8 Real part of the time domain Galileo E5 signal. (a) With 50 TECU ionospheric dispersion; (b) after using the blackman windowed sinc interpolation based ionospheric dispersion compensation method.

the proposed method is also discussed. The all-pass filter method is analyzed for comparison. The pilot component of Galileo E5 AltBOC(15,10) signal is used for the evaluation. For other BOC signals with high subcarrier rate, the results are the same so that they are not listed for simplicity.

Figure 8(a) illustrates the waveforms of the real part of the ideal AltBOC(15,10) baseband signal and the ionospheric dispersion deformed signal. Figure 8(b) shows the waveform after using the sinc interpolation based ionosphere compensation method to compensate the group delay dispersion. It shows that the time domain waveform is fluctuated and delayed with a corresponding time when the signal is traveling across the ionosphere. After the ionosphere is compensated by the proposed sinc interpolation based method, both of the fluctuation and the delay are nearly diminished.

Figure 9 draws the ionosphere induced power loss of the correlation results for different TEC and that after the ionospheric dispersion is compensated by the proposed method. It shows that the ionosphere will bring as large as 3 dB power loss when the TEC is larger than 150 TECU. With the help of the proposed sinc interpolation based method, the power loss is almost eliminated which is reduced to 0.01 dB.

In order to evaluate the code tracking bias after the ionosphere is compensated by the proposed method, the early minus late discriminator (EML) based DLL is considered here which is the usual choice in GNSS receiver. The EML makes use of the symmetry of the correlation function to synchronize the input code with the local one which is represented as

$$E_{\mathrm{EML}}(\tau,\delta) = R_{\mathrm{cf}}(\tau-\delta/2) - R_{\mathrm{cf}}(\tau+\delta/2), \tag{44}$$

where $R_{\mathrm{cf}}(\cdot)$ is the real part of the normalized CCF between the input baseband signal and the local reference signal. δ is the correlation space between the early branch (E) and late branch (L) and τ is the code phase bias. The code is regarded to be synchronized when the discriminator is zero. Hence, the code tracking bias is the τ when $E_{\mathrm{EML}}(\tau,\delta)=0$. Figure 10 illustrates the code tracking bias of different correlation space in the case that TEC is 50 TECU after the ionospheric dispersion is compensated with the proposed windowed sinc interpolation based method and the all-pass filter method. The parameters of the all-pass filter are TEC = 50 TECU, $N=23$ and $\beta=0.85$ according to [10]. The code tracking bias caused by ionospheric dispersion is also drawn for comparison in which the value is subtracted by 14.18 m that is the ionospheric delay at the Galileo E5 center frequency. It validates that the ionospheric dispersion can be compensated by the proposed method for the code tracking. Furthermore, the code tracking bias of the proposed method is smaller than the all-pass filter method which means that the proposed method can not only recover the BOC signal from ionospheric dispersion with high accuracy but keep the symmetry of the cross correlation function as well.

The proposed sinc interpolation based ionospheric dispersion compensation method also shows much lower complexity than the all-pass filter method. Considering the sinc interpolation is the convolution between the signal and the interpolation kernel which is the same as the process of filtering, the interpolation kernel size is equivalent to the filter order. The typical interpolation kernel sizes are 8 and 16 as

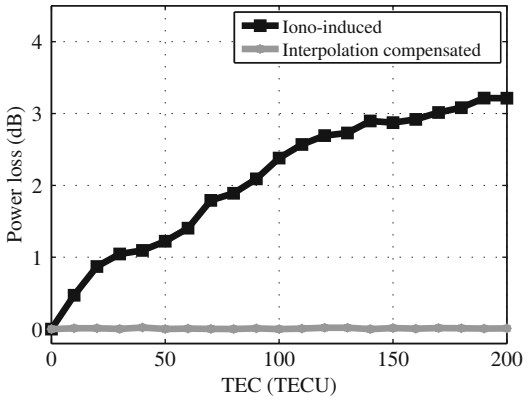

Figure 9 Ionosphere induced power loss and the power loss after compensated by the proposed blackman windowed sinc interpolation based method.

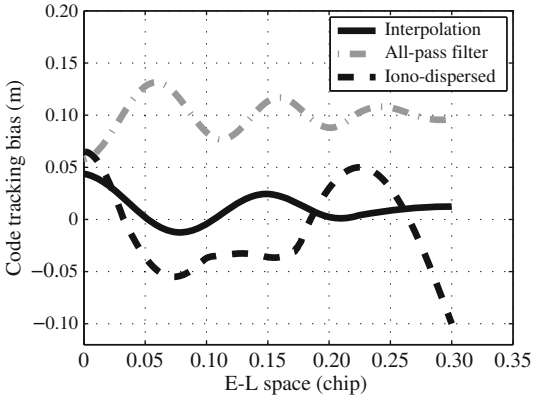

Figure 10 Code tracking bias of different E-L space. (The code tracking bias represented by the black dashed line is subtracted by 14.18 m).

the statement in Section 4 so that the equivalent order is only 8 or 16. The all-pass filter is composed of N second-order sub-filters [10]. According to the design example of the all-pass filter in [10], N is 23 so that the total order is 46. It is obvious that the sinc interpolation based method is much simpler than the all-pass filter method.

Furthermore, the value of TEC is time-varying and it may vary rapidly especially when ionosphere is perturbed. The parameter TEC utilized for the ionospheric dispersion compensation should be updated frequently so as to guarantee the compensation accuracy. For the sinc interpolation based method, the variation of the ionospheric dispersion induced by the varying TEC is comprised of two parts referring to (25) and (26). One of them is that over the intact sampling period. It is compensated by shifting the sampling points and no extra computational load is added. For the variation within the sampling interval, since the interpolation kernel size is fixed whose typical values are 8 and 16, only 8 or 16 points of sinc function value are needed to be calculated. Nevertheless, for the all-pass filter method, when TEC varies, the poles of the filter have to be replaced to minimize the compensation error. The large numbers of filter coefficients are needed to be calculated again according to the new poles. Additionally, the order of the filter is diverse for different TEC. The structure of the filter should also be changed when TEC varies. The process is really complex and brings huge computational costs which is nearly unrealizable in the real implementation. Therefore, the all-pass filter method often employs several fixed signal processing channels and each of them has the corresponding filter with the given TEC.

Figure 11 shows the code tracking bias of the EML based DLL when the ionosphere is compensated by the proposed sinc interpolation method and the all-pass filter methods with different number of signal processing channels. The E-L space of the EML is 0.3 chip. The ionosphere is compensated by the proposed sinc interpolation based method with the exact TEC which bring nearly no extra computational loads. Two kinds of all-pass filter groups are utilized to cover the TEC ranging from 0 TECU to 200 TECU for comparison. The mean square error between the group delay of the all-pass filter and the desired group delay over the signal band is around 10 according to [10]. The number of the filters used in the two groups are 4 and 8. Together with the channel without filter corresponding to the TEC of 0 TECU, the number of the signal processing channels is 5 and 9. The TEC intervals between the all-pass filters of the two groups are 50 TECU and 25 TECU respectively. The code tracking biases shown in the figure are the results that the ionosphere is compensated by the all-pass filter with the TEC closest to that of the signal. It is obvious that the ionospheric dispersion corresponding to all TEC can be compensated by the proposed method. But the bias of the all-pass filter method still can be close to 4m even when 9 channels are utilized which will highly degrade the positioning performance. Moreover, more computational loads are brought since multiple channels are employed. In consideration that each of the all-pass filters is more complex than the sinc interpolation, the filter group based all-pass filter method will lead to huge computational loads compared with the proposed sinc interpolation based ionospheric

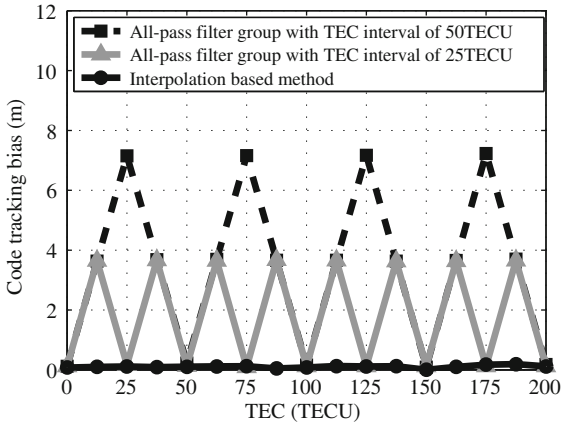

Figure 11 Code tracking bias after the ionospheric dispersion is compensated by the sinc interpolation based method and the all-pass filter groups.

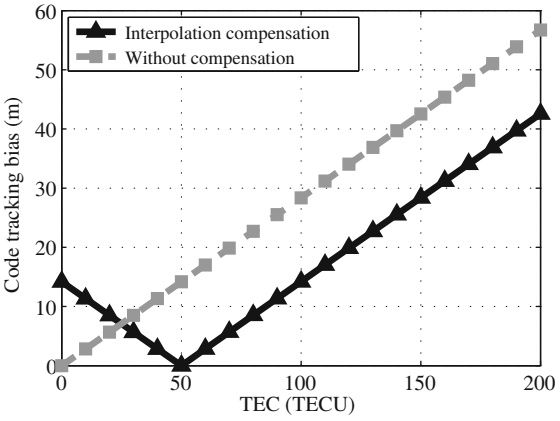

Figure 12 Code tracking bias before and after using the sinc interpolation based ionospheric dispersion compensation method with fixed TEC parameter of 50 TECU.

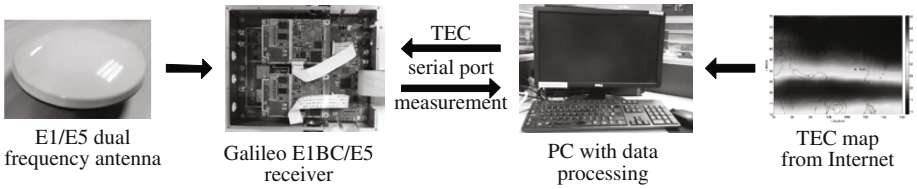

Figure 13 Real data test scheme.

dispersion compensation method.

Besides that, since TEC varies geographically and temporally, errors may exist in the measured TEC for the ionospheric dispersion compensation. Figure 12 draws the code tracking bias of the loop using the proposed sinc interpolation based ionospheric dispersion compensation method with fixed TEC parameter of 50 TECU under the assumption of different TEC for each dispersed input signal. The results without ionosphere compensation are also drawn. It informs that, when the TEC estimation error is as large as 20 TECU, the code tracking bias of the loop with the sinc interpolation based dispersion compensation is still smaller than that without compensation. When TEC is smaller than 20 TECU, it is over compensated and worse than that without compensation. When TEC is larger than 50 TECU, the code tracking bias after the compensation will increase as the TEC increases but it is always smaller than that without compensation. Since the error of the measured TEC, such as that extracted from the Global Ionospheric Maps broadcasted by Jet Propulsion Laboratory, is less than 1 TECU [24], the code tracking bias after the compensation is at most 0.28 m. Accordingly, the proposed sinc interpolation based method can almost completely compensate the ionospheric dispersion for BOC signals with high subcarrier rate.

In order to further evaluate the proposed ionospheric dispersion compensation method, real Galileo E5 data was used and a test was carried out. The data was taken under opened sky conditions from 12:30 pm to 9:00 pm local time on June 30, 2015 in Beijing. The real data test scheme is shown in Figure 13. The Galileo E5 signals are first collected using an E1/E5 dual frequency antenna, then transferred to a receiver executing the proposed sinc interpolation based ionospheric dispersion compensation method. In the receiver, there are several independent identical signal processing channels driven by the same clock. A third-order PLL, a second-order DLL and SLL with carrier aiding are utilized in each channel for the signal tracking. The bandwidths implemented are 15 Hz for the PLL and 0.5 Hz for the DLL and SLL. The EML with a narrow correlator spacing of 0.1 code chip is used. In the test, the Galileo E5 signals without ionosphere compensation are also processed in the identical loop at the same time for comparison. Besides the Galileo E5 signal, we also receive the Galileo E1BC signal to calculate the dual frequency pseudo range as the reference. The real time TEC is gained from the TEC map on the Internet and sent to the receiver for ionosphere compensation through serial port. Figure 14 shows the TEC during the test. It is relatively high at noon and reduces at night.

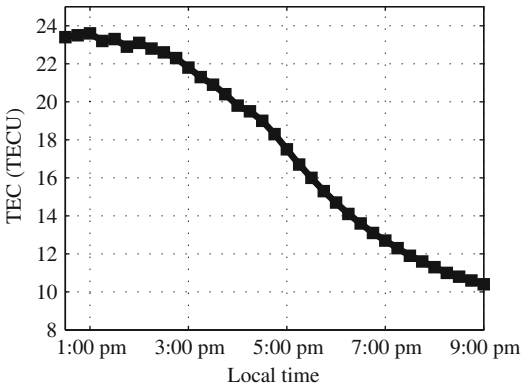

Figure 14 TEC during the test (Gained from the TEC map on the Internet).

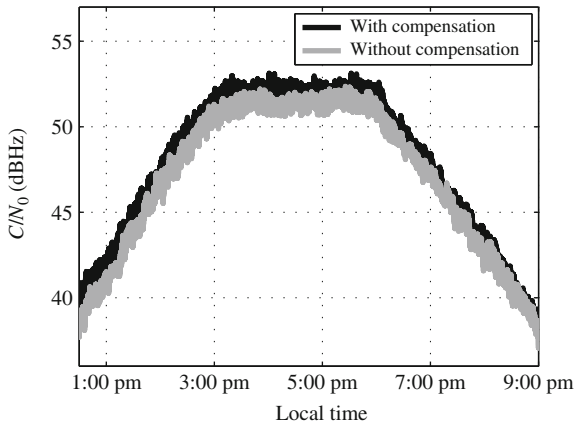

Figure 15 The estimated C/N_0 of SV11 with and without ionospheric dispersion compensation.

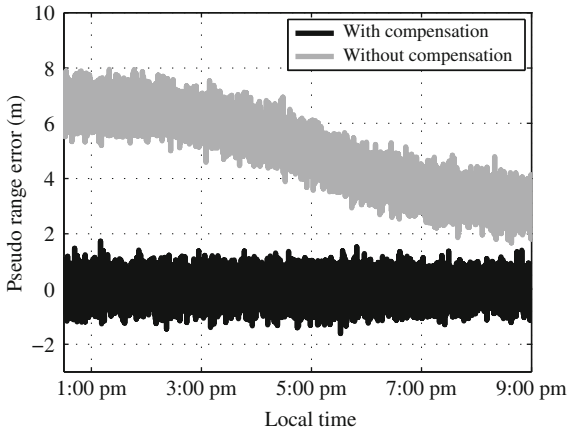

Figure 16 Pseudo range error of SV11 with and without ionospheric dispersion compensation.

During the test, the Galileo SV11 is received. The carrier to noise density ratio (C/N_0) of the E5 pilot signal of SV11 is estimated from the correlation outputs [13]. The C/N_0 estimation results of the E5 signal received with and without ionospheric dispersion compensation are drawn in Figure 15. It shows that the C/N_0 after ionosphere compensation is higher than that without compensation especially when TEC is high. Referring to Figure 9, it validate that the proposed method can effectively compensate the power loss induced by the ionospheric dispersion for BOC signal with high subcarrier rate. Furthermore, it also demonstrates that the sinc interpolation based method can perfectly compensate the ionospheric dispersion all the time when TEC is varying.

Additionally, the pseudo ranges calculated from the loop with the proposed sinc interpolation based ionospheric dispersion compensation and without compensation are recorded. The pseudo range of the satellite is also computed from the Galileo E1BC and E5a signal (the LSB of E5 signal). By compensating the ionosphere dispersion effects with the common dual frequency method, it is free of ionospheric dispersion and used as the reference for evaluation. The errors of the pseudo ranges that are calculated from the loops with and without ionosphere compensation are drawn in Figure 16.

It shows that, when the ionospheric dispersion is compensated by the proposed sinc interpolation based method, the pseudo range error varies around zero. However, if ionosphere is not compensated, there is a deviation existing in the pseudo range measurements besides the jitter induced by the noise. Since all of the signals are processed with the identical channels driven by the same clock and the pseudo range error is calculated by subtracting the E5 pseudo range from the E1BC/E5a dual frequency pseudo range extracted at the same time, according to the pseudo range formulation [23], all other deviations except that induced by ionosphere are diminished. The deviations in the pseudo range error shown in the figure is that caused by the ionospheric dispersion. Hence, the results validates that the ionospheric dispersion can be effectively compensated by the proposed method. Furthermore, the reference is the E1BC/E5a

dual frequency pseudo range whose error jitter is about 1m which is really large [25]. In fact, after the ionosphere is compensated by the proposed sinc interpolation based method, the pseudo range error jitter of E5 signal is much smaller than that shown in the figure. In addition, the result also confirms that, with the real time TEC, the proposed sinc interpolation based method can almost entirely compensate the ionospheric dispersion for BOC signal with high subcarrier rate in the case with varied TEC.

6 Conclusion

In this paper, the sinc interpolation based ionospheric dispersion compensation method for BOC signals with high subcarrier rate is proposed. Firstly, BOC signal is modeled as the sum of two side band signals which have the spectrum like the BPSK signal. Based on the model, the ionospheric dispersion deformed BOC signal is gained by delaying the phases of the two side bands according to the ionospheric dispersion effects. Subsequently, the sinc interpolation based method is developed to compensate the dispersion between the two side band signals. The performance of the proposed method is evaluated by comparing the time domain waveform, power loss and code tracking bias of the signal with those in the condition without ionosphere. It is also compared with the all-pass filter method. Furthermore, the real Galileo E5 signal data is collected and utilized to assess the proposed method. The results show that the proposed method can almost totally compensate the ionospheric dispersion effects on BOC signal with high subcarrier rate and the computational loads are much lower than the existing methods.

Acknowledgements This work was supported by National Natural Science Foundation of China (Grant No. 61101128) and 111 Project of China (Grant No. B14010)

Conflict of interest The authors declare that they have no conflict of interest.

References

1 Unite Nations. Current and planned global and regional navigation satellite systems and satellite-based augmentations systems. In: Proceeding of the International Committee on Global Navigation Satellite Systems Provider's Forum, New York, 2010. 15–40
2 Betz J W. Binary offset carrier modulations for radio navigation. Navigation, 2002, 48: 227–246.
3 Galileo Project Office. The GIOVE-A+B signal in space interface control document. European Space Agency, 2008
4 Christie J R I, Parkinson B W, Enge P K. The effects of the ionosphere and C/A frequency on GPS signal shape: considerations for GNSS-2. In: Proceedings of the 9th International Technical Meeting of the Satellite Division of The Institute of Navigation, Kansas City, 1996. 647–653
5 Yao Z, Lu M Q, Feng Z M. Unambiguous sine-phased binary offset carrier modulated signal acquisition technique. IEEE Trans Wirel Commun, 2010, 9: 577–580
6 Ren J W, Jia W M, Chen H H, et al. Unambiguous tracking method for alternative binary offset carrier modulated signals based on dual estimate loop. IEEE Commun Lett, 2012, 16: 1737–1740
7 Borio D. Double phase estimator: new unambiguous binary offset carrier tracking algorithm. IET Radar Sonar Nav, 2014, 8: 729–741
8 Martin N, Leblond V, Guillotel G, et al. BOC(x,y) signal acquisition techniques and performances. In: Proceedings of the 16th International Technical Meeting of the Satellite Division of The Institute of Navigation, Portland, 2003. 188–198
9 Gao G, Datta-Barua S, Walter T, et al. Ionosphere effects for wideband GNSS signals. In: Proceedings of the 63rd Annual Meeting of The Institute of Navigation, Cambridge, 2007. 147–155
10 Guo N Y, Kou Y H, Zhao Y, et al. An all-pass filter for compensation of ionospheric dispersion effects on wideband GNSS signals. GPS Solut, 2014, 18: 625–637
11 Klobuchar J A. Ionospheric time-delay algorithm for single frequency GPS users. IEEE Trans Aerosp Electron Syst, 1989, 23: 325–331
12 Lestraquit L, Artaud G, Issler J L. AltBOC for dummies or everything you always wanted to know about AltBOC. In: Proceedings of the 21st International Technical Meeting of the Satellite Division of The Institute of Navigation, Savannah, 2008. 961–970
13 Kaplan E D, Hegarty C. Understanding GPS: Principles and Applications. 2nd ed. Norwood: Artech House Publishers, 2005. 164–179, 233–234
14 Parkinson B, Spilker J J. Global Positioning System: Theory and Applications. Volume I. Washington DC: American Institute of Aeronautics and Astronautics, 1996. 489–490

15 Rebeyrol E, Macabiau C, Lestarquit L, et al. BOC power spectrum densities. In: Proceedings of the 2005 National Technical Meeting of The Institute of Navigation, San Diego, 2005. 769–778
16 Radicella S M, Nava B. NeQuick model: origin and evolution. In: Proceedings of the International Symposium on Antennas Propagation and EM Theory (ISAPE), Guangzhou, 2010. 422–425
17 Dooley S R, Nandi A K. Adaptive subsample time delay estimation using Lagrange interpolators. IEEE Signal Process Lett, 1999, 6: 65–67
18 Schanze T. Sinc interpolation of discrete periodic signals. IEEE Trans Signal Process, 1995, 43: 1502–1503
19 Cavicchi T J. DFT time domain interpolation. IEE Proc-F Radar Signal Proc, 1992, 139: 207–211
20 Dooley S R, Asoke K N. Notes on the Interpolation of discrete periodic signals using sinc function related approaches. IEEE Trans Signal Process, 2000, 48: 1201–1203
21 Lehmann T M, Gonner C, Spitzer K. Survey: interpolation methods in medical image processing. IEEE Trans Med Imag, 1990, 18: 1049–1075
22 Hodgart M, Blunt P. Dual estimate receiver of binary offset carrier modulated signals for global navigation satellite systems. Electron Lett, 2007, 43: 1–2
23 Misra P, Enge P. Global Positioning System: Signals, Measurements, And Performance. Lincoln: Ganga-Jamuna Press, 2001. 434–442, 482–492, 148–151
24 Kunitsyn V, Kurbatov G, Yasyukevich Y, et al. Investigation of SBAS L1/L5 signals and their application to the ionospheric TEC studies. IEEE Geosci Remote Sens Lett, 2015, 12: 547–551
25 Julien O, Macabiau C, Issler J L. Ionospheric delay estimation strategies using Galileo E5 signals only. In: Proceedings of the 22nd International Technical Meeting of The Satellite Division of the Institute of Navigation, Savannah, 2009. 3128–3141